Sensors and Materials, Vol. 37, No. 7 (2025) 2779–2791
MYU Tokyo

S & M 4086

Metallographic Classification Using Deep Learning Models

Chih-Yung Chen,[1] Nan Hua Lu,[2] and Rey-Chue Hwang[2*]

[1]Program of Artificial Intelligence and Mechatronics, National Pingtung University of Science and Technology, No. 1, Shuefu Road, Neipu, Pingtung 912301, Taiwan
[2]Department of Electrical Engineering, I-Shou University, No. 1, Sec. 1, Syuecheng Rd., Dashu District, Kaohsiung City 84001, Taiwan

(Received October 21, 2024; accepted May 9, 2025)

Keywords: deep learning, spheroidization, metallography

In this study, we explored deploying deep learning to control the steel spheroidization process and metallography determination. Utilizing raw material images, we refined parameters such as temperature for enhanced spheroidization stability, drawing on expert knowledge. Employing an extensive dataset, we tested the steel spheroidization process at 775 and 745 °C, comparing spheroidization levels with a 760 °C baseline. Our focus spanned preprocess metallography and post-spheroidization assessment, using the EfficientNet transfer learning model. Results revealed high accuracy in preprocess determination. For spheroidization rates, categorizing into two groups yielded a correctness rate of more than 95%, showcasing the model's proficiency in discerning metallographic characteristics.

1. Introduction

The steel industry, a cornerstone of heavy manufacturing, encompasses the production of various products spanning upstream, midstream, and downstream sectors. This sector, crucial for national economic development, faces challenges in global competition, necessitating improvements in product quality and value addition. Screws and fasteners, integral components across industries, highlight the steel industry's role in global economic infrastructure.[1,2] To address global competition challenges, metal industries are focusing on refinement, high unit prices, and increased value addition.

In conventional raw material plants, a small amount of chromium, molybdenum, and other elements is added to steel to significantly enhance its hardenability and mechanical performance. However, such low-alloy steels with chromium content contribute to a defect rate of 5–10% in the wire production of steel mills, thereby further escalating spheroidization costs.[3] In reality, optimal spheroidization is achieved through a process that reorganizes carbides in steel into finely distributed globular structures of cementite. The identical carbide composition and uniform distribution are essential for generating strengthening effects, ensuring the maximization of steel ductility and fatigue cracking. Therefore, in this study, we focused on the precise analysis and discussion of the metallography of spheroidized steel.

*Corresponding author: e-mail: rchwang@isu.edu.tw
https://doi.org/10.18494/SAM5403

ISSN 0914-4935 © MYU K.K.
https://myukk.org/

We explored the physical properties of spheroidization from a microscopic perspective, identifying differences between materials spheroidized normally and those with poor spheroidization. Leveraging advancements in artificial intelligence, particularly deep learning image recognition techniques, we aimed to evaluate metallographic images of fastener wire pre-spheroidization. The application of deep learning neural networks for metallographic assessment seeks to identify optimal parameters for setting spheroidization process temperatures, replacing traditional empirical settings.

2. Spheroidization

Spheroidization is an important annealing method in steel heat treatment,[2,3] which aims to achieve grain uniformity in the ferrite matrix. To optimize spheroidized steel materials, crucial factors include heating temperature range, deformation size, and isothermal holding time after deformation.[4,5] Adjustments based on temperature, time, gas, and processing methods are made before wire entry. Manual experience in setting temperatures during spheroidization results in a defect rate of 3–10%. Thus, we proposed a pre-spheroidization metallographic prediction method to reduce spheroidization defects in carbon alloy steels.

2.1 Metallographic analysis before spheroidization

In optimizing the spheroidization process, we determined that the metallurgical phase of the pre-spheroidization material significantly affects the choice of spheroidization process parameters. For typical medium-carbon hypoeutectoid steel alloys, pre-metallurgical phases fall into two major categories: coarse pearlite and fine pearlite. Fine pearlite is further subdivided into two phases: one with a clear, layered lamellar structure of snowflake-like cementite at grain boundaries and the other with a cloud-like, layered structure exhibiting less distinct fingerprint patterns. Figure 1 shows a difficult-to-spheroidize fine pearlite phase suitable for treatment at 775 ℃, whereas Fig. 2 shows a relatively easy-to-spheroidize phase suitable for treatment at 745 ℃. In this paper, we propose a metallographic identification system for pre-spheroidizing annealing to aid manufacturers in selecting optimal annealing temperatures, enhancing product yield and quality.[6]

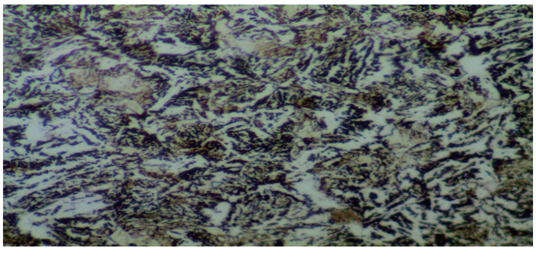

Fig. 1. (Color online) Difficult-to-spheroidize metallographic phase.

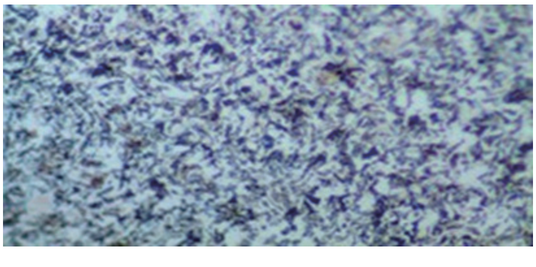

Fig. 2. (Color online) Easy-to-spheroidize metallographic phase.

2.2 Spheroidization metallographic grade

The contemporary demand for fastener processes is progressively advancing in complexity, exemplified by ISO898-1 Grade 12.9 specifications. High-grade fasteners find common utility in applications necessitating resilience to elevated strength and pressure. In forming or cold forging, fastener wires often encounter 70–80% deformation, underscoring the imperative to augment material ductility and hardness. Spheroidization, particularly for high-carbon steels such as eutectoid and hyper-eutectoid, is undertaken to mitigate hardness, refine structural morphology, and enhance plasticity and machinability. Hence, spheroidization annealing treatment is necessary for almost all alloy steel fasteners with sub-eutectoid compositions. The assessment of spheroidization rates is conventionally executed through standard chart comparison and digital image analysis. Standard chart comparison entails aligning spheroidization outcomes with established charts to derive the rate, while digital image analysis employs image processing techniques for automated rate calculation. Spheroidization rate judgment adheres to prevalent standards such as Japanese Industrial Standards (JIS), American Society for Testing and Materials (ASTM), and other regulatory norms. These standards evaluate and categorize spheroidization results on the basis of organizational characteristics, rate, and pertinent factors.[7] Taking ASTM F 2282-03 as an instance, we show the metallographic image of grade 1 to grade 4 spheroidized metal in Fig. 3.

2.3 Digital image analysis

Digital image analysis, utilizing computer vision, is employed to calculate the spheroidization rate in metallurgical studies. Two methodologies are utilized for this calculation. The first method involves using particles as the basis for determining the length-to-width ratio of carbide particles meeting specific conditions. Equation (1) expresses the spheroidization rate (*S.R.*), where N_p represents the count of particles with an aspect ratio below 5 and N_{Total} is the overall sampled particle count. The second method employs area as the unit for evaluating the carbide area ratio meeting length–width criteria to the total sampling area, as depicted in Eq. (2), where

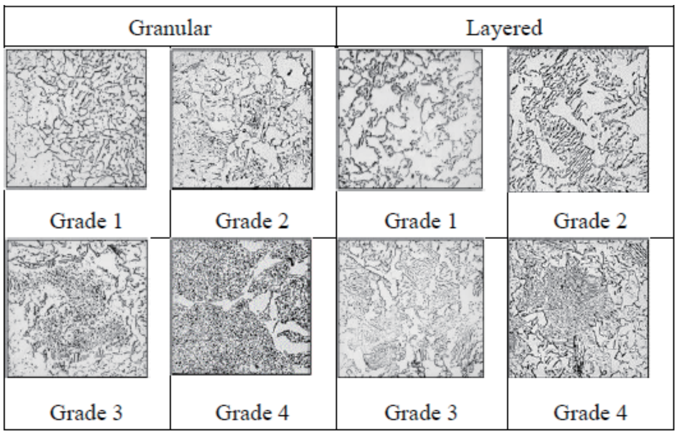

Fig. 3. ASTM F 2282-03 standard metallographic diagram.

$S.R.$ is the spheroidization rate, A_P is the aspect ratio for areas below 5, and A_{Total} is the total sampling area.

$$S.R. = \frac{N_P}{N_{Total}} \times 100\% \quad (1)$$

$$S.R. = \frac{A_P}{A_{Total}} \times 100\% \quad (2)$$

Metallographic analysis is integral to materials science, enabling the microscopic scrutiny of material structures. This facilitates the elucidation of elemental compositions and physical/mechanical properties after various processing treatments. Metallographers identify processing techniques enhancing material properties, thereby elevating product quality and reliability. For instance, Chen used metallography to scrutinize magnesium alloys and observe corrosion reactions in diverse solutions and under varying heat treatments, aiming to bolster corrosion resistance.[8] Kuo utilized metallography to explore grain distribution in magnesium alloys after different annealing treatments and tension tests at varying temperatures.[9]

2.4 Examining cracks from a microstructural perspective

By investigating the microstructure of the cold forging process, valuable insights into the impact of material composition and processing on performance and structure are gained. In contrast to conventional macroscopic analyses, we delved into microstructural patterns to identify potential defects, as depicted in Fig. 4. The analysis of chemical composition aids in optimizing material performance, positively affecting product quality.[10] Figure 4 shows screws with production defects undergoing microstructural examination; red-circled areas indicate a bainitic structure. According to Ref. 10, smaller carburized particles enhance metal ductility. In this study, we verified that the microstructural pattern shown in Fig. 4(a) can reduce the number of cold forging cracks in subsequent processing, whereas the microstructural pattern shown in Fig. 4(b) leads to cracks, as shown in Figs. 5 and 6, confirming the proposed perspective.[10]

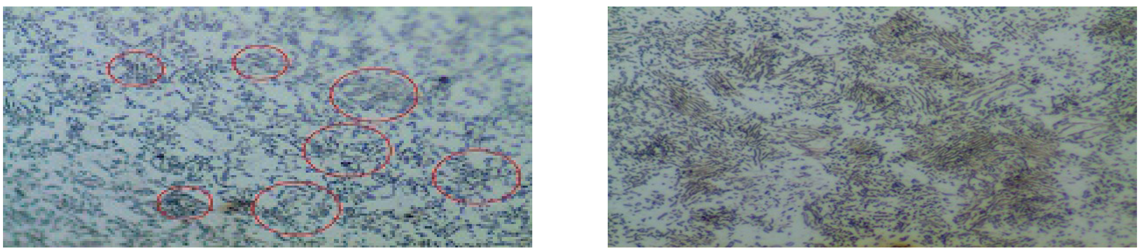

(a) (b)

Fig. 4. (Color online) Poor spheroidization proportion chart. (a) Metallurgical structure less likely to produce defective products. (b) Metallographic structure that easily produces defective products.

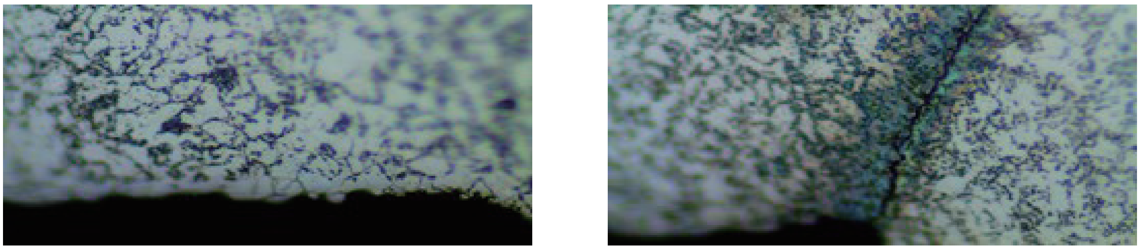

Fig. 5. (Color online) Cracks caused by subsequent cold forging of poorly spheroidized steel.

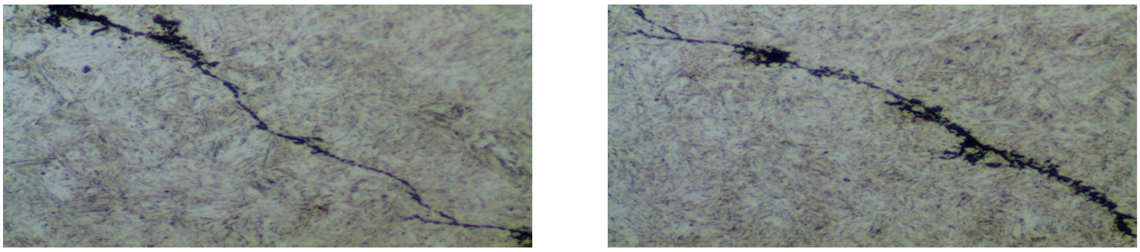

Fig. 6. (Color online) Cracks caused by subsequent quenching of poorly spheroidized steel.

3. Research Methods

3.1 Deep learning and convolutional neural networks (CNNs)

The rapid advancement of deep learning technologies has brought forth new perspectives and methodologies in various research domains, particularly in the realm of image recognition. The application of CNNs has proven beneficial for the analysis of metallography, a technique investigating the relationship between the structure and properties of metallic materials. CNNs, widely employed in image classification, object detection, and related fields, serve as the focal point of this study. The objective is to explore the efficacy of CNNs in metallography and subsequently optimize the network model to enhance the precision and efficiency of metallographic analysis. In this paper, we present an overview of the principles of CNNs and their application in metallography.(11–14) We delve into how this model can be utilized for metallographic analysis and material structure design. Our aim is to provide novel insights and methodologies for the field of metallography and its associated domains through this research.

3.2 Study methods

Before processing into fasteners, post-spheroidized metal wires undergo metallographic inspection to prevent waste. The spheroidization degree is typically examined to ensure compatibility with subsequent processes. Currently, metallographic tests are conducted after spheroidization to guarantee fastener production quality. Producing noncompliant wires after spheroidization depletes resources. In this study, we aim to establish a classification model for post-spheroidized metal wires and determine suitable spheroidization process temperatures before production, minimizing defective steel material production. The methodology includes pre- and postproduction steel metallographic inspections in two stages: determining spheroidizing temperature before spheroidization and grading steel spheroidization based on the metallography of the steel after spheroidization. Artificial intelligence, specifically EfficientNet, is employed for image processing and intelligent model development based on images collected before and after manufacturing.

3.2.1 EfficientNet and its structure

In the realm of deep learning applications, it is well established that augmenting the depth of a model (ResNet[15]) can yield more complex and suitable feature information during data learning, while increasing the width of a model (MobileNets[16]) often enables the extraction of finer data features within the same feature map. Employing high-resolution input images allows for a detailed extraction of information from the input data.

However, concurrently modifying the depth, width, and resolution of a model makes it challenging to precisely quantify the impact on model accuracy. As a result, the majority of research primarily focuses on investigating the effects of these adjustments in a singular direction. Tan and Le asserted the existence of a specific proportional relationship among the depth, width, and resolution of CNN models.[17] They experimentally quantified these three variables, contending that the uniform scaling of depth, width, and resolution using a set of fixed coefficients leads to a more precise and effective model architecture. Consequently, they proposed a novel approach called compound model scaling and utilized this concept to formulate the EfficientNet model architecture.

The EfficientNet model architecture incorporates the mobile inverted bottleneck convolution, which adopts the linear bottleneck concept from Mobilenetv2[18] and the notion of inverted residuals, building upon the depth-wise separable convolutions from lightweight MobileNet.[16] This design aims to reduce parameter usage effectively. EfficientNet begins by establishing a baseline model (EfficientNet-B0) and subsequently extends to other model structures (EfficientNet-B1 through B7) through a methodology known as compound scaling, as proposed in Ref. 17. This approach involves uniformly scaling the baseline model's depth, width, and resolution by certain proportions using the coefficient ψ, as illustrated in Eq. (3). Here, d, w, and r represent scaling factors for depth, width, and resolution, respectively. ψ denotes the scaling coefficient, and the constraint $\alpha \cdot \beta^2 \cdot \gamma^2 \approx 2$ ensures that the computational cost floating-point operations per second (FLOPs) increases by a factor of 2^{ψ} after each scaling operation. In Ref. 18, a grid search method was employed to determine the optimal values for α, β and γ, which were found to be 1.2, 1.1, and 1.15, respectively.

The model architecture and parameter configuration of EfficientNet-B0 are illustrated in Fig. 7. To generate the model architecture for EfficientNet-B1, set ϕ to 1, producing scaling factors for

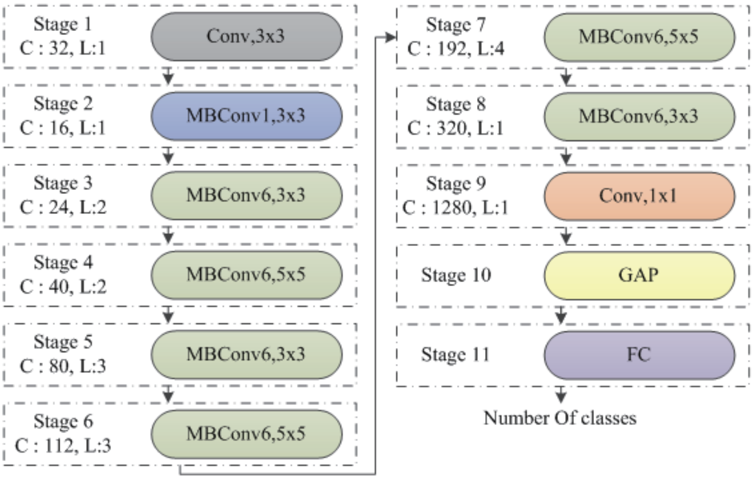

C: Channel, L: Layer, FC: Fully Connected, GAP: Global Average Pooling

Fig. 7. (Color online) EfficientNet-B0 structure.

depth, width, and resolution. Subsequently, multiply the depth, width, and resolution of EfficientNet-B0 by the corresponding scaling factors to achieve the desired EfficientNet-B1 model architecture.

$$\begin{aligned} &depth : d = \alpha^{\psi}, width : w = \beta^{\psi}, resolution : r = \gamma^{\psi} \\ &\text{s.t. } \alpha \cdot \beta^2 \cdot \gamma^2 \approx 2, \alpha \geq 1, \beta \geq 1, \gamma \geq 1 \end{aligned} \tag{3}$$

3.2.2 First phase of study

The first phase of the study involved determining the temperature of the spheroidization process using the microstructure of the as-processed steel. On the basis of our empirical knowledge, we collected 20 images of the microstructure of steel that spheroidizes hardly and 20 images of steel that spheroidizes easily. Subsequently, these two types of steel were divided into two groups, each consisting of 10 images, and subjected to spheroidizing treatment at temperatures of 745 and 775 °C. Table 1 shows the grading results after spheroidizing treatment for both types of steel. From Table 1, it can be observed that for steel that is difficult to spheroidize, the optimal treatment temperature is 775 °C, whereas for steel that spheroidizes easily, the appropriate treatment temperature is 745 °C.

The microstructural examples for treatments at 745 and 775 °C are illustrated in Figs. 8(a) and 8(b). Figures 9(a)–9(d) present corresponding diagrams for different microstructures subjected to appropriate and inappropriate spheroidizing temperatures. From the metallographic analysis following experimentation, it is evident that the spheroidization grade of the microstructure significantly improves after suitable temperature spheroidizing treatment.

Table 1
Statistical results of two steel types after spheroidizing treatment.

Steels prone to spheroidization			Steels more prone to spheroidization		
No.	745 ℃	775 ℃	No.	745 ℃	775 ℃
1	Grade 2	Grade 1	1	Grade 2	Grade 3
2	Grade 3	Grade 2	2	Grade 1	Grade 4
3	Grade 4	Grade 1	3	Grade 1	Grade 3
4	Grade 3	Grade 1	4	Grade 2	Grade 3
5	Grade 4	Grade 2	5	Grade 2	Grade 3
6	Grade 3	Grade 2	6	Grade 1	Grade 3
7	Grade 3	Grade 2	7	Grade 2	Grade 4
8	Grade 3	Grade 1	8	Grade 2	Grade 3
9	Grade 4	Grade 2	9	Grade 2	Grade 4
10	Grade 3	Grade 2	10	Grade 1	Grade 3

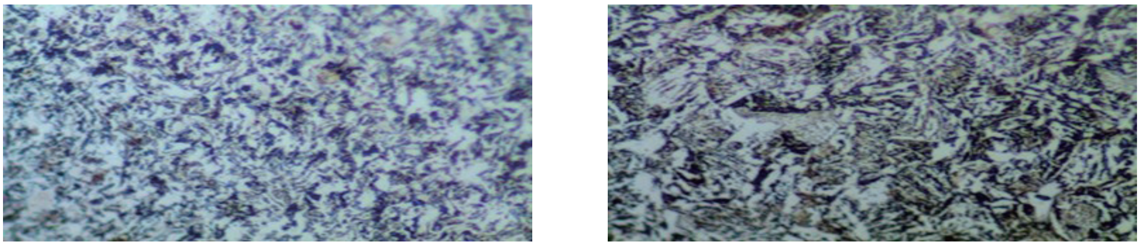

(a) (b)

Fig. 8. (Color online) Metallographic type before process. (a) Suitable for processing at 745 ℃. (b) Suitable for processing at 775 ℃.

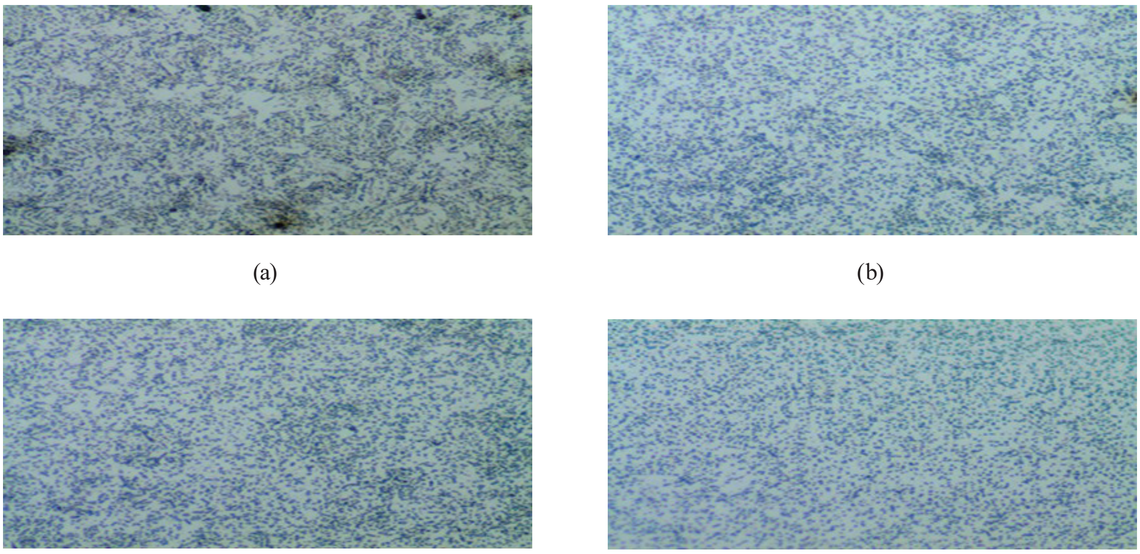

(a) (b)

(c) (d)

Fig. 9. (Color online) Corresponding diagrams for different microstructures subjected to appropriate and inappropriate spheroidizing temperatures. (a) Suitable for 745 ℃ but use 775 ℃ spheroidization. (b) Suitable for 745 ℃ and use 745 ℃ spheroidization. (c) Suitable for 775 ℃ but use 745 ℃ spheroidization. (d) Suitable for 775 ℃ and use 775 ℃ spheroidization.

3.2.3 Second phase of study

The second phase of the study needs to utilize spheroidized metallographic images and the judgment of quality control personnel on spheroidization results as training and testing datasets. Quality control personnel primarily employ the ASTM F 2282-03 standard to assess spheroidization rates, which are categorized into four grades. The collection of images for each grade and their distribution in terms of quantity are presented in Table 2.

4. Experiments

During our research, to achieve objectivity and enhance model performance with limited data, we employed a fivefold cross-validation approach. Specifically, we randomly split all images in a 3:1 ratio, with 75% designated as the training set and 25% as the testing set. In the experimental phase of our study, we compared three feature extraction models, namely, EfficientNet-B0, EfficientNet-B1, and EfficientNet-B2. For each model, we selected the weights that yielded the highest accuracy in testing as the evaluation criteria. This approach allowed for a comprehensive assessment of each model's performance, facilitating the selection of the optimal model for subsequent applications.

4.1 Spheroidizing temperature classification

In this study, regarding the temperature classification in the spheroidization process, we collected a total of 200 images, that is, 100 images of steel suitable for 775 °C treatment and 100 images of steel suitable for 745 °C treatment. We randomly divided these images into five sets (G1 to G5) of training and testing data in a 3:1 ratio. The category distribution for each set of training and testing data is presented in Table 3. Table 4 shows the training and testing results of the three models, and their temperature classification accuracies can almost reach 100%.

Table 2
Quantity distribution of various image types.

Spheroidization rate	Number of images
Grade 1	106
Grade 2	97
Grade 3	92
Grade 4	96

Table 3
Training and testing data distribution of images before spheroidization.

	Training	Testing
745 °C	75	25
775 °C	75	25
Total No.	150	50

Table 4
Temperature classification accuracies of the three models on the G1-G5 training and testing datasets (%).

Training data	G1	G2	G3	G4	G5
EfficientNet-B0	99	100	100	100	99
EfficientNet-B1	99	100	99	100	99
EfficientNet-B2	99	100	100	99	100
Testing data	G1	G2	G3	G4	G5
EfficientNet-B0	100	100	100	100	100
EfficientNet-B1	100	100	100	100	100
EfficientNet-B2	100	100	100	100	100

Table 5
Category distribution of training and testing sets.

	No. of training	No. of testing
Grade 1	79	27
Grade 2	72	25
Grade 3	69	23
Grade 4	72	24

Table 6
Accuracy of metallographic grading for training and testing datasets (%).

Training data	G1	G2	G3	G4	G5
EfficientNet-B0	87	89	90	90	91
EfficientNet-B1	88	90	86	88	87
EfficientNet-B2	85	89	90	86	90
Testing data	G1	G2	G3	G4	G5
EfficientNet-B0	89	92	90	87	88
EfficientNet-B1	89	91	90	86	87
EfficientNet-B2	88	90	89	87	88

Table 7
Accuracy of judgments performed using EfficientNet-B0 model (100%).

	G1	G2	G3	G4	G5
Training data	94.50	95.21	96.58	96.58	96.92
Testing data	96.97	97.98	96.97	95.96	95.96

4.2 Metallographic grading of spheroidization

In this study, we collected 391 images with different grades of spheroidization processing, as shown in Table 2. The category distribution of the training and testing sets is shown in Table 5. To better train the model and evaluate its performance, we randomly divided these images into five sets (G1–G5) of training and testing sets in a 3:1 ratio for each image type. This distribution ensures that the class distributions in the training and testing sets are similar while also reducing the bias caused by category imbalance. Through this distribution of datasets, the model can learn features of various image types and can accurately classify and detect different image types.

From the accuracy of the training and testing datasets in Tables 4 and 6, it is observed that all three models from EfficientNet-B0 to EfficientNet-B2 indeed have achieved good performance.

In spheroidization detection, specifically, a metallographic spheroidization grade of 1 or 2 indicates compliance with quality standards, whereas a grade of 3 or 4 indicates failure to meet standards. Therefore, when conducting the spheroidization test, we focus on the situation where an image rated 1 or 2 is misclassified as 3 or 4, and vice versa. To evaluate the performance of the model, we considered ratings of 1 and 2 as qualified and ratings of 3 and 4 as disqualified. Only EfficientNet-B0 was used in this study because it has the fewest parameters and performed well in previous studies. Table 7 illustrates the accuracy of judgments of qualification and disqualification on 292 training images and 99 testing images.

5. Conclusions

In view of the importance of the spheroidization quality of steel on metal products, we investigated the temperature control during steel spheroidization and the metallographic evaluation of steel after spheroidization using deep learning techniques. For the pre-process of steel spheroidization, we utilized metallographic images and employed a deep learning approach to refine temperature control parameters. A comparison was made between the metallographic characteristics before and after spheroidization, demonstrating that suitable temperature control enhances the stability of the spheroidization quality. We conducted tests at 775 and 745 ℃ using the collected metallographic dataset and employed the EfficientNet transfer learning model to evaluate the pre-spheroidization and post-spheroidization metallography. The results showed a high correlation between pre-treatment temperature control and metallographic quality. In determining the spheroidization rate of the steel, the accuracy rate for both qualified and failed metallographic classifications exceeded 95%, illustrating the proficiency and practicality of the deep learning model in identifying metallographic features.

Although the EfficientNet transfer learning model demonstrated commendable performance in this study, several practical limitations must be thoroughly considered to enable comprehensive application. For example, in terms of computational cost, training EfficientNet models typically requires significant computational costs. Large datasets necessitate high-performance hardware, and scaling to massive and diverse datasets further increases training time and memory requirements. In terms of industrial applicability, in industrial environments, adopting EfficientNet may face challenges such as inference latency, which can hinder real-time applications. In terms of specialized hardware requirements, EfficientNet achieves optimal performance on high-end hardware. Deploying it in resource-constrained environments, such as IoT devices, may lead to suboptimal outcomes.

In future research, we believe that the reliability of the study can be significantly enhanced with the collection of more metallographic datasets. Furthermore, exploring the use of simple models with few parameters could be a valuable avenue for improving the accuracy of metallographic evaluation while also reducing the model training and execution time.

Acknowledgments

This research was supported by the Ministry of Science and Technology, Taiwan, under contract No. MOST 113-2221-E-214-015.

References

1 K. Lu: Science **328** (2010) 319. https://doi.org/10.1126/science.1185866
2 I. C. Hung, W. Hsieh, and S. M. Kuo: China Steel Tech. Rep. **34** (2021) 29. https://www.csc.com.tw/csc_c/ts/ena/pdf/no34/pages/5-Development%20of%20Pre-heating%20Spheroidization%20technology%20for%20Cr-added%20Low%20Alloy%20Steel.pdf
3 M. Umar, F. Qayyum, M. U. Farooq, S. Guk, M. Kirschner, G. Korpala, and U. Prahl: Steel Res. Int. **93** (2022) 2100452. https://doi.org/10.1002/srin.202100452
4 B. Mašek, H. Jirková, and L. Kučerová: Mater. Sci. Forum **706** (2012) 2770. https//doi.org/10.4028/www.scientific.net/MSF.706-709.2770
5 V. A. Alza: IOSR J. Mech. Civil Eng. **18** (2021) 63. https://doi.org/10.9790/1684-1803036381
6 E. Karadeniz: Mater. Des. **29** (2008) 251. https://doi.org/10.1016/j.matdes.2006.11.015
7 ASTM F2282-23 Standard Specification for Quality Assurance Requirements for Carbon and Alloy Steel Wire, Rods, and Bars for Mechanical Fasteners, standard by ASTM International, 11/01/2023. https://store.accuristech.com/standards/astm-f2282-23?product_id=2576740 (accessed June 2024).
8 H. P. Chen: The influence of microstructure on the corrosion behaviors of die-cast AZ91D magnesium alloy, Master Thesis, Department of Materials Science and Engineering, National Cheng Kung University, Taiwan (2002).
9 C. Y. Kuo: Effects of rotary swaging and annealing on mechanical properties of AZ series magnesium alloys, Master Thesis, Department of Materials Science and Mineral Resource Engineering, National Taipei University of Technology (2011).
10 A. Monden, K. Miyanishi, S. Yamasaki, and T. Ochi: Nippon Steel Tech. Rep. **103** (2013) 127. https://www.nipponsteel.com/en/tech/report/nsc/pdf/103-20.pdf
11 A. A. K. Farizhandi, and M. Mamivand: Mater. Des. **219** (2022) 110799. https://doi.org/10.1016/j.matdes.2022.110799
12 Y. Xu, Y. Zhang, M. Zhang, M. Wang, W. Xu, C. Wang, Y. Sun, and P. Wei: Sensors **21** (2021) 43. https://doi.org/10.3390/s21010043
13 L. Che, Z. He, K. Zheng, T. Si, M. Ge, H. Cheng, and L. Zeng: Mater. Today Commun. **37** (2023) 107531. https://doi.org/10.1016/j.mtcomm.2023.107531
14 Q. Zhao, J. Kang, and K. Wu: Metals **14** (2024) 732. https://doi.org/10.3390/met14060732
15 K. He, X. Zhang, S. Ren, and J. Sun: Proc. 2016 IEEE Int. Conf. Computer Vision and Pattern Recognition (IEEE, 2016) 770. https://doi.org/10.1109/CVPR.2016.90
16 A. G. Howard, M. Zhu, B. Chen, D. Kalenichenko, W. Wang, T. Weyand, M. Andreetto, and H. Adam: arXiv preprint arXiv:1704.04861 (2017). https://doi.org/10.48550/arXiv.1704.04861
17 M. Tan, and Q. V. Le: Proc. 2019 Int. Conf. Machine Learning (2019) 6105. https://doi.org/10.48550/arXiv.1905.11946
18 M. Sandler, A. Howard, M. Zhu, A. Zhmoginov, and L. C. Chen: Proc. 2018 IEEE Conf. Computer Vision and Pattern Recognition (IEEE, 2018) 4510. https://doi.org/10.48550/arXiv.1801.04381

About the Authors

Chih-Yung Chen received his B.S and M.S. degrees in computer science and information engineering from Tamkang University in 1998 and 2000, respectively, and his Ph.D. degree in electrical engineering from I-Shou University in 2008. Currently, he is an associate professor at the Program of Artificial Intelligence and Mechatronics, National Pingtung University of Science and Technology, Taiwan. His research interests are in the areas of artificial intelligence, autonomous robot control, database system, and software engineering.
(mikechen@mail.npust.edu.tw)

Nan Hua Lu received his Ph.D. degree in electrical engineering from the Electrical Engineering Department of I-Shou University, Taiwan, in 2023. His research interests include image processing, neural network, and fuzzy theory. (nahua@livemail.tw)

Rey-Chue Hwang received his Ph.D. degree in electrical engineering from Southern Methodist University, Dallas, TX, in 1993. Currently, he is a full professor at the Electrical Engineering Department of I-Shou University, Taiwan, R.O.C. He has published more than 300 papers in various journals and conferences in the areas of artificial intelligence systems, signal processing, and fuzzy control. He is now a fellow of IET and a senior member of IEEE. He chartered the IEEE CIS Chapter, Tainan Section, and served as the co-chair and chair from 2004 to 2009. (rchwang@isu.edu.tw)